Dynamic Electrochemical Membranes for Continuous Affinity Protein Separation

*Zhiqiang Chen, Tao Chen, Xinghua Sun, and Bruce. J. Hinds**

A membrane system with nanometer-scale thick electrodes is able to selectively bind genetically modified proteins and pump them across the membrane with sequential voltage pulses. The electrodes are located at the first 20 nm of pore entrances to specifically capture targeted proteins and block non-specific protein transport through the pores during the binding cycle. During the release cycle, concentration of imidazole is controlled to keep the pore blocked while releasing proteins at the bottom edge of the electrode. A separation factor for GFP:BSA of 16 was achieved with observed GFP electrophoretic mobility of 2.54×10^{-6} cm^2 V^{-1} s^{-1}. This non-optimized system with a membrane area of 0.75 cm^2 has the same throughput as 1 mL of commercially available chromatography columns showing viability as a continuous process. This system will enable continuous separation of expressed proteins directly from fermentation broths dramatically simplifying the separation process as well as reducing bio-pharmaceutical production costs.

1. Introduction

Genetic modification of a host cell to produce complex biomolecules is the critical route to bio-pharmaceutical production.[1–3] However, the separation of the desired protein from the myriad in living systems is the most costly and complicated step. The high cost of downstream purification of genetic protein expression hinders the wide-spread use of therapeutic protein treatments with an example prophylactic replacement therapy being greater than $100 000 per patient per year. Even with current advances in automated separation technology, 80% of the total cost of urokinase production is in purification.[4] The ability to genetically add poly-histidine tags to recombinant proteins enables affinity purification by immobilized metal ion affinity chromatography (IMAC),[5] which is the dominate separation method. However, IMAC suffers from limitations of long intra-particle diffusion time, high pressure drops, difficulties in packing large columns, column regeneration, non-specific binding, high cost and long binding/purge cycles.[6] The ideal separation method would be to have a selective membrane that could actively pump selected proteins across a barrier in a continuous process. Traditional polymeric ultrafiltration membranes have been studied for protein separation/purification,[7,8] however pore size is difficult to control and manipulate, leading to modest selectivity between similar proteins. Track-etching membranes and porous alumina membranes have precise pore size[9,10] and Au plating has been successfully used to tune pore size surface chemistry, and electrochemical activity.[11–13] In complex mixtures, many classes of proteins have similar size and surface charge, making selectivity an ongoing challenge. Indiscriminate fouling induced by flow is still a major limitation in pressure driven membrane separation that needs to be addressed.[14] Applied electric field, instead of pressure across the thick nanoporous membranes[15–17] have shown enhanced rates and result in rough charge-density based separation. Ultrathin silicon membranes with ≈10 nm thickness and 5 nm pore size have even been developed and show potential for protein separation[18] due to short path length and tight pore size distribution. However separations based principally on the basis of size and/or charges are not sufficient to isolate specific proteins from complex cell extracts. Affinity nanoporous membranes with immobilized ligands within the pores have the ability to capture highly specific proteins from cell extracts. However the operation is similar to IMAC, requiring binding/release cycles.[19] Compared to IMAC, the membrane have more efficient flowing mass transport to binding sites but several orders of magnitude less binding area. [20]

Biological membranes are capable of selectively transporting chemicals at dramatically enhanced rates with precise chemical selectivity and thus bio-inspired membranes have various applications in sensing, drug delivery and chemical separations.[21–24] To mimic this natural biological system, the membrane platform should have receptor chemistry at the pore entrances acting as gatekeeper that can specifically capture and concentrate the target protein, and have a driving force to pump the protein across the membrane barrier. Here we report an active membrane system based on nm-scale electrodes that allow voltage pulses for sequential affinity protein binding and release/pumping cycles. In particular the pore entrance is designed to bind target proteins, during both cycles, which block the pore from undesired protein transport across the membrane.

Z. Chen, T. Chen, Dr. X. Sun,[+] Prof. B. J. Hinds
Department of Chemical and Materials Engineering
University of Kentucky
Lexington, KY 40506, USA
E-mail: bjhinds@engr.uky.edu
[+]Present Address: Department of Bioengineering, University of Louisville, Louisville, KY 40292, USA

DOI: 10.1002/adfm.201303707

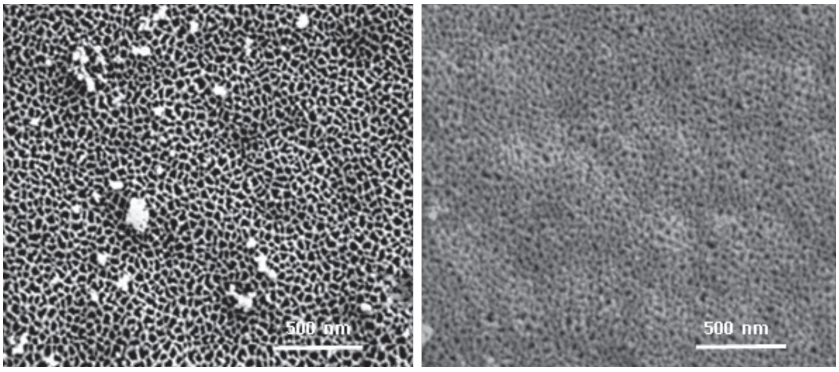

Figure 1. SEM images of AAO membrane (left) and with electro-less plated Au on top surface (right) to control the pore entrance sizes.

2. Results and Discussion

The primary active area of this protein separation system is the nm-diameter electrode coated pore at the membrane entrance that is matched to the dimensions of proteins (≈4 nm). This allows bound his-tagged proteins to block the pore from non-selective protein transport of a complex mixture. Shown in **Figure 1** is a scanning electron microscopy image of porous anodic aluminum oxide (AAO) membrane. Cross-sectional SEM images shows that the bare AAO membranes are asymmetric with a bulk pore structure comprised of 200 nm diameter straight channels and a thin porous layer at the top with a diameter of 27 nm.[25] The top and bottom membrane surfaces are coated with 5 nm of Au using sputtering deposition. This Au acts as a seed layer for the subsequent Au electro-less plating at the pore entrance region to reduce pore diameter to 10 nm by controlling plating time (Supporting Information Figure S1). The distance of the gold electrode down into the pore is also important since if the affinity chemistry is along the entire length of the pore, protein transport would be blocked by bound proteins. The sputtering process, that is not line-of-sight, would be expected to deposit Au roughly about 20 nm (pore diameter) down the pore length allowing 3–5 layer proteins to be bound along the channel. Nα,Nα-Bis(carboxymethyl)-L-lysine (NTA) was covalently grafted onto the gold electrode by electrochemical oxidation of the primary amine as depicted in **Figure 2**,[26] which is more resilient than thiol-Au analog.[27] Cyclic-voltamograms of the grafting process showed increased surface resistance (Supporting Information Figure S2,S3) confirming successful grafting. To demonstrate selective pore blockage by his-tagged green fluorescence protein (His-GFP) and subsequently releasing of His-GFP by imidazole, the electrophoretic fluxes of BSA before His-GFP binding, with bound His-GFP and after imidazole releasing are shown in **Figure 3**. BSA was used to simulate complex protein mixtures, since having the same polarity as His-GFP, it represents the biggest challenge in electrophoretic-based separations. A seven-fold decrease of BSA flux was seen in the blocked case and recovered to 95% of the original flux after imidazole release of bound His-GFP. **Table 1** shows the flux of His-GFP and BSA

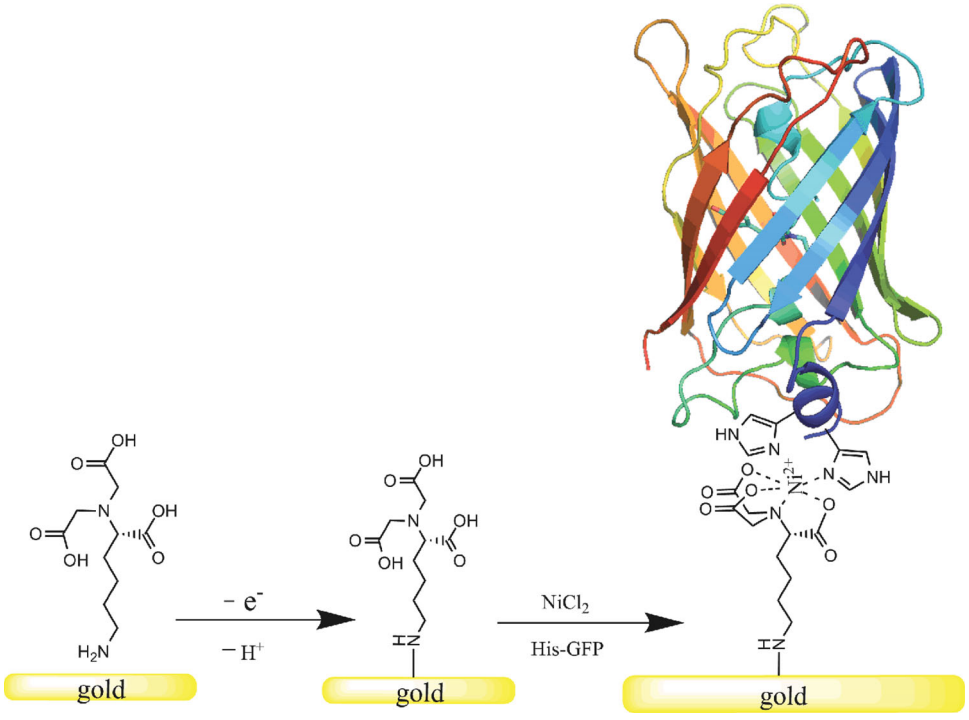

Figure 2. Schematic of N$_\alpha$,N$_\alpha$-Bis(carboxymethyl)-L-lysine electrochemical oxidation to functionalize gold layer and chelation bonding between NTA-Ni^{2+} and His-GFP

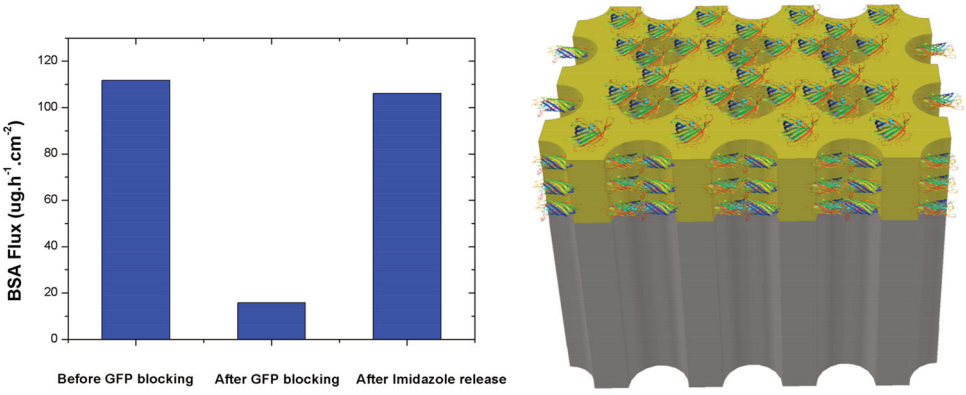

Figure 3. a) Electrophoretic pumping flux of BSA through functionalized AAO membrane before, after his-tagged GFP blocking, and after imidazole release of His-GFP (1000 μg mL^{-1} BSA feed concentration). b) Schematic of AAO membrane blocked by his-tagged GFP pore and protein size drawn to appropriate scale.

mixture (1:1) as a function of imidazole release agent. At high imidazole concentrations (10 mM) no binding/blocking was seen and both proteins are pumped through and no preferential separation was seen. At 1 mM imidazole partial blockage was seen with reduction in flux and modest selectivity. With the lowest imidazole (0.1 mM) concentration both GFP and BSA fluxes were markedly reduced (factor of 3.4 and 30 respectively) and a selectivity of 7.7 was seen. Two important inferences can be made from these series: 1) In the monolayer case, the release of a His-GFP leaves an open pore. The next event has a 50% chance of BSA to passing through pore or 50% chance of another His-GFP to block pore and be the next release event. This would give a maximum separation factor of 1 to 1.5, while 7.7 was observed. This indicates that more than a monolayer of His-GFP is at the pore entrance with near continuous blockage; 2) selective binding of His-GFP within pore, though enriching His-GFP, dramatically slows the flux, giving an inherent trade-off in flux versus. selectivity that is only exasperated with dilute target concentrations found in common separations.

The ideal separation system would be a two-cycle process, with binding step followed by transport step, mimicking the function of cell wall transporters. This can be achieved with electrophoretic pulses described in **Figure 4** with 2 two-electrode pairs system (Supporting Information Figure S4). During the first binding cycle, a small positive bias was applied on top Ni-NTA/gold surface to attract anionic His-GFP and repel imidazole from the binding surface and pumps it back to the permeate side. The second electrode pair, outside of the regenerated cellulose membrane, applies a large voltage to pump cationic imidazole from permeate side to the binding sites to release bound His-GFP as well as pump the released anionic His-GFP across the membrane to the permeate side. **Figure 5** shows the fluorescence spectra of feed and permeate solutions, showing the selective transport of His-GFP and a near background level signal of BSA. The results of the pumping study are summarized in **Table 2**. The first data column shows the control experiment with no binding chemistry and using only electrophoretic pumping (step 2). In this case both proteins have high flux, comparable mobility, and lack of selectivity due to open channels. In the second continuous electrophoretic pumping case, there is binding chemistry at the entrance and 10 mM of cationic imidazole in the permeate side that is pumped towards the binding site. In this case the pumping rate decreased due to binding chemistry at the pore entrance thus reduced pore size but no selectivity is seen since both proteins are electrophoretically pumped through the membranes. For the pulse pumping experiments in Table 2 we used a 0.05 V, 1s pulse for binding and a 0.3 V, 14s pulse for pumping. In this case a significant increase in His-GFP flux was seen and a selectivity of 9.2 was observed. It should be pointed out that this experiment had 100 fold higher BSA concentrations than His-GFP to more accurately simulate complex separations. In such a case there is a 100-fold higher probability of BSA entering an open pore entrance after His-GFP is released. The high separation factor indicates that the pore remains largely blocked, stopping BSA flux during the pumping cycle. In the fourth data column, a 1:1 ratio of BSA/His-GFP is used to reduce the probability of BSA entering opened pore and selectivity is thus raised to 16, showing the validity of the active pumping separation system. The pumping cycle time of 14s was based on a conservative estimate of the required amount of imidazole routinely used in IMAC to elute His-GFP[28] being be the molar equivalent of 150 mM times the AAO membrane volume (1.9×10^{-3} cm^3). With a 0.3 V measured potential drop across membrane electrodes (60 um) and the experimentally observed

Table 1. Electrophoretic flux and Mobility of Texas red conjugated BSA and His-GFP through Ni-NTA-Gold/AAO membrane with different imidazole concentration in permeate side.

Imidazole concentration [mM]	10	1	0.1
BSA flux [μg h^{-1} cm^{-2}]	0.30	0.12	0.01
His-GFP flux [μg h^{-1} cm^{-2}]	0.28	0.19	0.082
BSA effective mobility [10^{-6} cm^2 s^{-1} V^{-1}], μ_b	1.97	0.79	0.07
His-GFP effective mobility [10^{-6} cm^2 s^{-1} V^{-1}], μ_g	1.88	1.27	0.54
Selectivity, $S = \mu_g/\mu_b$	0.95	1.6	7.7

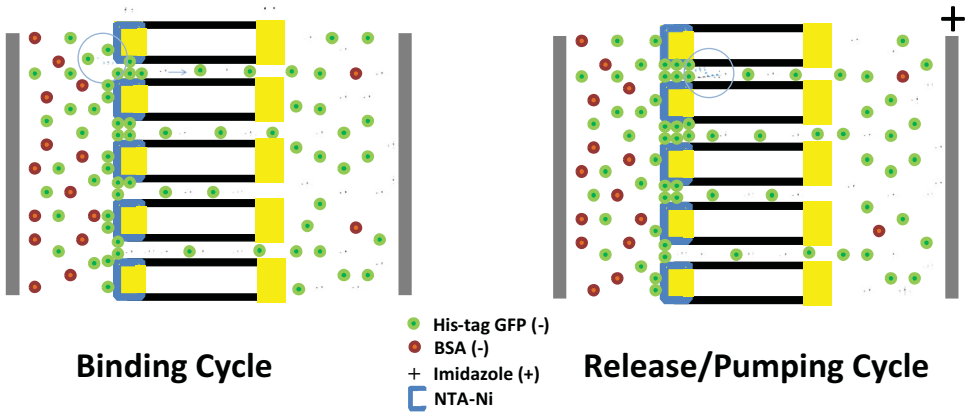

Figure 4. Schematic of pulsed electrophoresis 2-step process to pump His-tagged proteins across functionalized anodic aluminum membrane.

imidazole mobility of 14.4×10^{-5} cm^2 s^{-1} V^{-1} (see experimental section) an imidazole flux of 7.2×10^{-8} mol cm^{-2} s^{-1} is calculate from the 10 mM permeate solution, thus requiring 12.5 s to give 150 mM equivalent in the pore volume. To improve efficiency of pumping cycle, a valid model needs to be developed to predict imidazole concentrations at the pore entrance for each cycle.

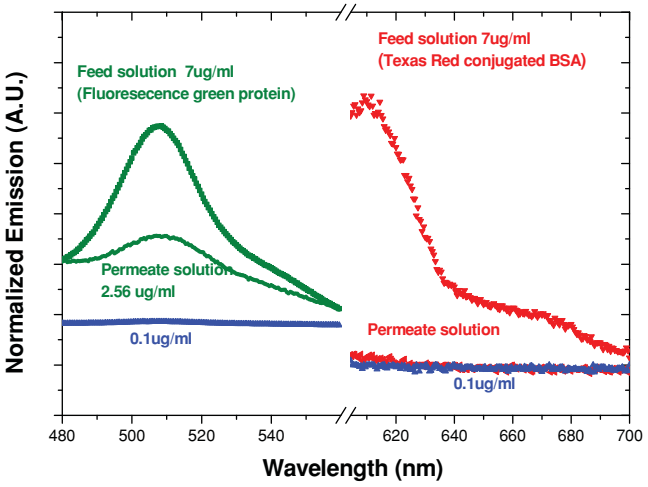

Figure 5. Fluorescence spectra showing the emission intensity of the baseline solutions, feed solutions, and permeate solutions after pulse electrophoresis.

The active membrane system is best modeled with a three-step process of 1) diffusion of the target to binding site from feed solution 2) pumping of imidazole from 'permeate' to release the target and 3) electrophoretic pumping of the target to the permeate. The three processes can be simulated numerically in 1 dimension by a combination of Fick's 1st law of diffusion and electrophoretic pumping:

$$J = D\frac{\Delta c}{\Delta x} + \mu E c \tag{1}$$

where J is flux per unit area, c is concentration, D is diffusion coefficient, μ is mobility, E is the electric field and Δx is the step width of simulation cell size (0.5 um).

The concentration change in the calculation cell is given by

$$\Delta c = J_{in} \times \Delta t \times \varepsilon_{rel} / \Delta x - J_{out} \times \Delta t \times \varepsilon_{rel} / \Delta x \tag{2}$$

where Δt is numerical simulation time step (5×10^{-5} s). J_{in} is flux (per unit area) in from neighbor cells and J_{out} flux out to neighbors calculated from Equation 1. Here, ε_{rel} is the relative porosity of calculation cell with respect to neighbor cell. AAO membranes are asymmetric with 3% porosity at the protein bound site and 60% porosity in the membrane open pore structure. Pore size is shrinking as we approach the 20 nm active pores and we would normally expect increasing electric field due to increased resistance of a smaller conducting cross-sectional

Table 2. Electrophoretic mobility and flux of BSA and His-tagged GFP proteins as a function of electrophoretic pumping cycle.

Pumping type	Gold/AAO membrane, direct pumping[a)]	Gold/AAO membrane, direct pumping[a)]	Ni-NTA-Gold/AAO membrane, pulse pumping [a)]	Ni-NTA-Gold/AAO membrane, pulse pumping [b)]
BSA flux [μg h^{-1} cm^{-2}]	112.56	48.32	14.07	0.02
His-GFP flux [μg h^{-1} cm^{-2}]	0.73	0.34	1.29	0.32
BSA effective mobility [10^{-6} cm^2 s^{-1} V^{-1}], μ_b	6.24	2.64	0.78	0.16
His-GFP effective mobility [10^{-6}cm^2 s^{-1} V^{-1}], μ_g	4.08	1.92	7.2	2.54
Selectivity, $S = \mu_g/\mu_b$	0.65	0.73	9.23	16

[a)]Feed solution contains 1000 μg mL^{-1} BSA and 10 μg mL^{-1} His-tagged GFP; [b)]Feed solution contains 7 μg mL^{-1} Texas red conjugated BSA and 7 μg mL^{-1} His-tagged GFP. The imidazole concentration in the permeate side is 10 mM.

area. However, due to the electrophoretic pumping of imidazole into a smaller volume, the ion concentration increases the conductivity of the solution thereby reducing electric field proportionately. Therefore we used constant electric field across the membrane in this simplified model. At the boundaries between feed solution, protein binding site, and open membrane channels, the difference of net protein flux due to changes in porosities, leads to the accumulation of imidazole at the binding site during electrophoretic pumping. Details of the Visual Basic simulation parameters are in the experimental section. Shown in **Figure 6**A–C are simulation of feed solution (0–30 μm), binding site (30.0–30.5 μm), bulk membrane (30.5–90 μm), and the permeate solutions (90–120 μm). Figure 6A shows the 1 second binding cycle depleting the target protein from feed solution following Ficks law of diffusion. This results in 0.0033 μg of protein absorbed onto the 0.32 cm^2 membrane area per 1s cycle. Most importantly, Figure 6A also shows the repulsion of imidazole at the binding site allowing target protein binding. The initial concentration of imidazole ($t = 0$) was the steady state profile after 1 cycle. Figure 6B shows the numerical simulation of the release/pumping cycle. The imidazole is quickly pumped to a steady-state profile of high concentrations at the binding site. According to Equation 2, the concentration increase at the binding side is primarily due to reduction in porosity from bulk pore side (60%) to the binding site (3%). The drop in imidazole concentration into the feed (at 0.003 cm) is primarily a result of the abrupt change in porosity. This simplified model used 0 mM imidazole at 0 um as a boundary condition to represent a bulk solution sink, but the concentration at this point would increase with pumping time to near the imidazole source concentration. However, most important is modulating the imidazole concentration near the pore entrance (sub-micrometer scale). In the binding cycle, the imidazole is electrostatically pushed away from pore entrance (Figure 6A) and does not require a strong concentration gradient to the bulk value 0 mM to achieve this.

For the protein pumping, the pore is blocked by bound proteins at pore entrance, thus only pumping of the sterically bulky target towards the permeate (to the right) can occur. Depending on the release rate after imidazole accumulation, the concentration of protein in pores can exceed feed solution. In this case, the protein was released at 12 s and electropohoretically pumped into the channel. During the next pumping cycle, that peak would be pumped to the permeate for the full 14s of the cycle. Figure 6C shows the predicted concentration profiles after 10 full cycles at the end of release/pumping cycle. Most important is that the first protein peak is pumped away from the binding site with cycle 2 and a steady state profile develops. With its higher mobility, the imidazole concentration profile achieves steady state by the end of the first cycle.

For the third step of pumping protein across the membrane, the observed His-GFP mobility across AAO membrane was 1.92×10^{-6} cm^2 s^{-1} V^{-1}, roughly 75-fold slower than imidazole (14.4×10^{-5} cm^2 s^{-1} V^{-1}). Under 50 V cm^{-1} field, the protein transit time across 60 um thick membrane is 62.5 s. However, it is important to point out that the target protein does not have to exit the membrane during each cycle, but be removed far enough from the binding site so as to not be pumped back during the binding cycle, as seen in Figure 6C. The pumping distance of the target protein within the pore channel is directly proportional to the electric field times pumping duration. In our case a factor of 6 for electric field and 14 for pumping time would decrease the backwards pumping length during binding

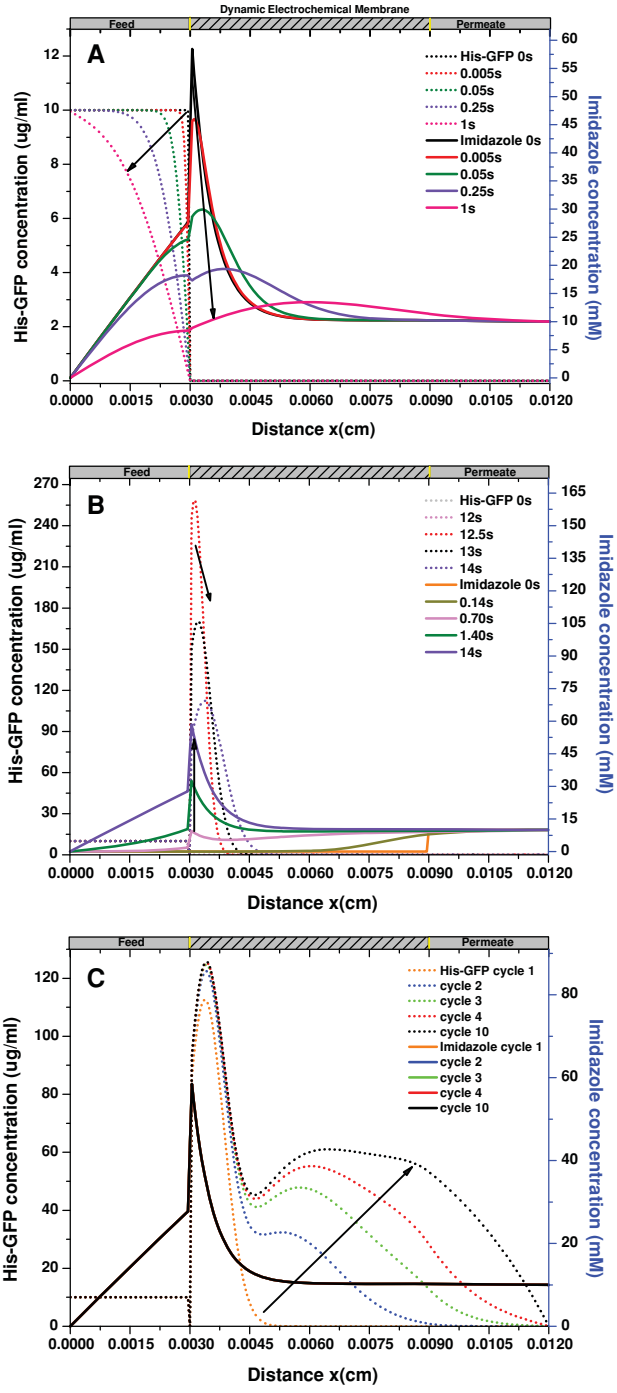

Figure 6. Numerical simulation results of the pulse pumping cycles: A) His-GFP binding and imidazole repulsion concetration during the 1 s diffusion/repel cycle +0.05 V at top electrode (x = 30 um); B) His-GFP pumping and imidazole accumulation concentration profile during the 14 s releasing/pumping cycle (50 V cm^{-1} across simulation); C) His-GFP and imidazole concentration profile at the end of pumping/releasing cycle as a function of total cycle number. Imidazole profiles all overlap under cycle 10.

cycle by a factor of 84 compared to the forward pumping cycle. Our 1 s/14 s binding/pump cycle times was chosen from the estimates of the first two steps. Decreasing the overall cycle time can increase pumping rate proportionally, however require the knowledge of release rate kinetics, which is the object of future study. At present, this technique is not suitable for cationic proteins with extreme pI. Large increases in pH (>pI), to render the protein anionic, would likely agglomerate protein mixtures. An alternative binding system with anionic release agent would have to be used for cationic proteins to ensure opposite electrophoretic pumping direction. Also with complex Cell lysate mixtures, additional pre-filtering or an addition membrane protection layer would likely be required to prevent non-specific binding or agglomerate fouling.

Overall pumping efficiency can be calculated from the observed His-GFP (4.5 μg) collected in permeate divided by the calculated His-GFP captured (0.0033 μg) times number of 1s binding cycles (2640 cycles) giving 51.7% efficiency. This is also consistent with the premise that bound protein at the entrance is required to block the pore during pumping of released target. This non-optimized system can be directly compared to commercial IMAC columns (calculations in Supporting Information) where this system requires 0.75 cm^2 of membrane area to have the same through put as a 1 cm^3 IMAC column used for laboratory scale separations. With optimization of binding/release pulse cycle amplitude/duration and electrode geometry, a promising active separation system from continuously producing bio-systems can be realized.

3. Conclusion

In conclusion, commercially available AAO membranes were successfully functionalized to mimic biological membranes for efficient protein separation. His-tagged proteins bound to the pore entrance block other proteins in a sequential/hopping manner, allowing selective transport during a release cycle. Electrophoretic pumping eliminates fouling associated with pressure flow, while pores closed by gatekeeper prevent fouling by other charged proteins. Pulsed electrophoresis binding/release/pumping cycle allows for a continuous protein separation process with low cost and high productivity. This would revolutionize protein separations where expressed proteins can be directly removed from fermentation baths with this membrane separation system.

4. Experimental Section

Reagents and Materials: 20 nm Anodic Aluminum Oxide (AAO) membranes (60 um thick) were obtained from Whatman (GE Healthcare). These AAO membranes are asymmetric with a bulk pore structure comprised of 200 nm diameter straight channels and a thin porous layer at the top with a diameter of 27 nm. The porosity was ≈60%. Gold (I) thiosulfate (Alfa Aesar) was used to electro-less deposit gold electrodes at the entrance and exits of these membranes. NiCl2, Nα, Nα-Bis(carboxymethyl)-L-lysine (Sigma Aldrich) and Ascorbic acid (EM Science) were used as received. Bovine serum albumin (BSA, pI = 4.9, MW = 67 000) was purchased from Sigma Aldrich and used as received. Texas red conjugated BSA was purchased from Life Technologies Aldrich and used as received. His-tagged green fluorescence protein (His-GFP, pI = 5.7, MW = 28 000) was obtained from Millipore and used as received. Purified water was prepared using a Millipore Milli-Q water purification system with 18.0 MΩ cm resistivity. Regenerated cellulose membranes (molecular weight cutoff 3500) were purchased from Spectrum Laboratories, Inc. These regenerated membranes were rinsed with water for 1 h to remove glycerine before use.

Gold Electrodes/AAO Membrane Preparation: Gold sputtering was first performed to create gold seed for the gold electro-less plating. Sputtering was performed with a Cressington Coating System (Ted-Pella) with calibrated quartz crystal monitor with background pressure of 0.02 mbar at 100 W power. No intermediate wetting layer (i.e., Ti/TiO_2) on Al_2O_3 was needed for seeding the Au layer. 5 nm gold was sputtered on both the entrance and exit of AAO membranes at 1 nm min^{-1} gold sputtering rate, which would deposit approximate the diameter (20 nm for the entrance and 200 nm for the exit) distance down the pore length. The gold Electro-less plating reactions will only form on the sputtered gold seed layer. Electro-less plating[29] was accomplished in 50 mM pH 7.0 phosphate buffer containing 1.6 mM sodium gold (I) thiosulfate and 2.68 mM ascorbic acid. The reaction is given by

$$C_6H_8O_6 \rightarrow C_6H_6O_6 + 2e^- + 2H^+ \quad (3)$$

$$Au(S_2O_3)_2^{3-} + e^- \rightleftharpoons Au + 2S_2O_3^{2-} \quad (4)$$

The pore size can be tuned by controlling the electro-less plating time. For larger pores the AAO membrane pore entrance size was measured by the analysis of images from a Hitachi S-4300 Scanning Electron Microscope (SEM). For smaller pores, the diameter was measured by flux of distilled water across the membrane under constant pressure and calculated using Hagen-Poiseuille equation.

Gold Electrodes/AAO Membrane Functionalization: As-prepared gold/AAO membranes were covalently grafted with Nα,Nα-Bis(carboxymethyl)-L-lysine (NTA, Sigma Aldrich) by electrochemical oxidation.[26] The electrochemical grafting was performed in 0.1 M $LiClO_4$ ethanol solution with 10 mM NTA (Figure S2, Supporting Information). Five cycles of the cyclic voltammogram scans from 0 V to 1.2 V (10 mV s^{-1} scan rate) showed a reduction in the 0.83 V oxidation peak as the electrode became more conductive (Figure S2, Supporting Information). After electrochemical oxidation grafting, a cyclic voltammograms of 0.1 M in $K_3Fe(CN)_6$ in 0.1 M PHOSPHATE solution (PH = 7) was carried out to show increased surface resistance from grafting (Figure S3, Supporting Information). The membrane was then thoroughly rinsed using de-ionized water and ethanol to dissolve any byproducts after the electrochemical oxidation grafting. The membrane was finally incubated in 0.1 M $NiCl_2$ (Sigma Aldrich) for 30 min to form conjugate Ni-NTA surface. The chelate binding between Ni-NTA and His-tagged GFP is diagrammed in Figure 2.

Bulk Mobility of GFP and Mobility of Imidazole Across the AAO Membrane: The bulk mobility of GFP (7×10^{-5} cm^2 s^{-1} V^{-1}) at PH 7 was measured by using a particle-size and zeta-potential analyzer (Beckman Coulter Delsa Nano C Particle Analyzer) at 25 °C. The experimental mobility of imidazole across the AAO membrane was studied using the setup in Figure S4 without the waveform generator. First a four-point standard curve of imidazole was drawn based on the 280 nm UV-vis adsorption of imidazole at different concentrations. The imidazole mobility (μ) at PH 7 then can be determined by $\mu = \frac{J}{E \times C}$, where J is the imidazole flux across the AAO membrane; E is the electric field across the AAO membrane and C is the feed imidazole concentration. The calculated imidazole mobility through AAO membrane is 14.4×10^{-5} cm^2 s^{-1} V^{-1}.

Protein Separation Experiments: Two model proteins used for separation are His-GFP and BSA. His-tagged GFP has eleven strands on the outside of cylinders form the walls of the structure. The cylinders have a diameter of 30 Å and a length of 40 Å. BSA is also a cylinder with a diameter of 55 Å and a length of 90 Å. The setup for protein pumping process was shown in Figure S4, Supporting Information. In direct electrophoretic pumping, only the potentiostat (EA164 QuadStat, eDAQ

Pty Ltd), which is controlled by an e-corder 410 (eDAQ Pty Ltd) with Chart software, was used and placed on the outer cells. Two Pt wires (one connected to the working electrode and the other one connected to the counter and reference electrode) were connected to the potentiostat and inserted into the outer electrolyte phosphate buffer (50 mM, PH = 7) solutions. Two regenerated cellulose membranes (3500 MW cuttoff) were used in the to isolate the proteins, BSA (67,000 Daltons) and GFP (28,000 Daltons), from the high voltage (6 V) of the pumping cycle electrodes. At PH 7, both GFP and BSA were negatively charged. The anode was in the phosphate buffer adjacent to the permeate solution so that the negative charged proteins will be electrophoretically pumped to the permeate solution and the positively charged imidazole will be electrophoretically pumped to the feed solution from the permeate solution. When a 6 V was applied by the potentiostat to Pt electrodes in outer cell, the voltage drop directly measured across the gold electrodes/AAO membrane was 0.3 V, accounting for a large system resistance. Water underwent electrolysis and generated H^+ in the anode and OH^- in the cathode at 6 V in the outer compartments and phosphate buffer was changed frequently to maintain the PH during the water electrolysis process. The volume of feed solution was ~1 ml and the permeate solution was ≈0.5 mL. The feed solution contained 7 μg mL^{-1} Texas red conjugated BSA and His-tagged GFP and the permeate solution contained 0.1–10 mM imidazole. In the pulse electrophoretic pumping process, a waveform generator (Keithley 3390 arbitrary waveform generator) was also used to generate 0.05 V across the Au/AAO/Au membrane during the binding cycle with electrodes directly connected to top and bottom Au layers. This is contrasted against the EA164 QuadStat potentiostat used to generate 6 V bias across the entire system resulting in a 0.3 V drop across Au/AAO/Au membrane during the release/pumping cycle. The feed solution contained 1) 7 μg mL^{-1} Texas red conjugated BSA and His-tagged GFP (1:1) or 2) 1000 μg mL^{-1} BSA and 10 μg mL^{-1} His-tagged GFP (100:1); and the permeate solution contained 10 mM imidazole.

Protein Assay Methods: The fluorescence intensity of His-GFP was measured using a fluorescence spectrophotometer (PerkinElmer LS 55 Fluorescence spectrometer), with an excitation filter of 395 nm and an emission filter of 509 nm. The fluorescence intensity of Texas red conjugated BSA was measured with an excitation filter of 596 nm and an emission filter of 615 nm. The fluorescence intensities of the experimental samples were compared to the five–point standard curves of His-GFP and Texas red conjugated BSA. In the 1000 μg/ml BSA and 10 μg/ml His-tagged GFP purification experiment, the total protein in the feed and permeate solution was expressed in mg/mL and compared with total protein concentrations expressed as BSA at λ = 280 nm in a spectrophotometer. The 5-point BSA standard curve for the permeate solution was based on UV-vis adsorption of BSA at 280 nm in 10 mM imidazole solution to account for imidazole spectral overlap with BSA. The total protein concentrations in the permeate solution ranged from 50 to 1000 μg mL^{-1}.

Numerical Modeling of Protein Pumping Membrane System: Microsoft Excel with Visual Basic Macros was used to numerically calculate concentrations in the model system. A matrix of 240 *x*-axis values (0–120 μm, 0.5 um steps) was initialized with boundary conditions and starting profiles. A new matrix was made for the new time (previous time + time step). Flux to/from neighbor cells into new matrix were calculated using Equation 1. The concentration change in the cell can be calculated from the flux of Equation 2 using the values in the matrix of the prior time step. After calculating each new concentration at x location, the prior time step matrix is overwritten with the newly calculated matrix and the cycle repeated until desired total time is reached using "For/Next" loops. Time steps were chosen to be such that $(D\,\Delta t)^{0.5} + c\,E\,\mu\,\Delta t$ (characteristic diffusion length + electrophoretic distance) was much less than Δx (typically $0.1\Delta x$ to ensure numerical accuracy and stability. Detail physical parameters in the model can be found in the Supporting Information.

Supporting Information

Supporting Information is available from the Wiley Online Library or from the author.

Acknowledgements

The authors thank the Center for Nanoscale Science and Engineering for critical infrastructure. This work was supported by NIH NIDA, #5R01DA018822–05 and DARPA, W911NF-09–1–0267.

Received: October 31, 2013
Revised: January 13, 2014
Published online: April 16, 2014

[1] G. Walsh, *Nat. Biotechnol.* **2010**, *28*, 917.
[2] B. Leader, Q. J. Baca, D. E. Golan, *Nature* **2008**, *7*, 21.
[3] A. K. Pavlou, J. M. Reichert, *Nat. Biotechnol.* **2004**, *22*, 1513.
[4] R. Ghosh, Z. F. Cui, *J. Membrane Sci.* **2000**, *167*, 47.
[5] E. K. M. Uedaa, P. W. Goutb, L. Morgantia, *J. Chromatogr.A.* **2003**, *988*, 1.
[6] Q. Luo, H. Zou, X. Xiao, Z. Guo, L. Kong, X. Mao, *J. Chromatogr. A.* **2001**, *926*, 255.
[7] B. Cheang, A. L. Zydney, *J. Membrane Sci.* **2004**, *231*, 159.
[8] A. L. Zydney, *Int. Dairy J.* **1998**, *8*, 243.
[9] H. U. Osmanbeyoglua, T. B. Hurb, H. K. Kimb, *J. Membrane Sci.* **2009**, *343*, 1.
[10] E. L. Savariar, K. Krishnamoorthy, S. Thayumanavan, *Nat. Nanotechnol.* **2008**, *3*, 112.
[11] K. B. Jirage, J. C. Hulteen, C. R. Martin, *Science* **1997**, *278*, 655.
[12] S. Yu, S. B. Lee, M. Kang, C. R. Martin, *Nano Lett.* **2001**, *1*, 495.
[13] K. Y. Chun, P. Stroeve, *Langmuir* **2002**, *18*, 4653.
[14] I. H. Huisman, P. Prádanos, A. Hernández, *J. Membrane Sci.* **2000**, *179*, 79.
[15] J. Wu, K. Gerstandt, H. Zhang, J. Liu, B. J. Hinds, *Nat. Nanotechnol.* **2012**, *7*, 133.
[16] S. Yu, S. B. Lee, C. R. Martin, *Anal. Chem.* **2003**, *75*, 1239.
[17] X. Sun, X. Su, J. Wu, B. J. Hinds, *Langmuir* **2011**, *27*, 3150.
[18] C. C. Striemer, T. R. Gaborski, J. L. McGrath, *Nature* **2007**,*445*, 749.
[19] P. Jain, M. K. Vyas, J. H. Geiger, G. L. Baker, M. L. Bruening, *Biomacromolecules* **2010**, *11*, 1019.
[20] R. Ghosh, *J. Chromatogr. A* **2002**, *952*, 13.
[21] S. W. Kowalczyk, *Trends Biotechnol.* **2011**, *29*, 608.
[22] E. C. Yusko, J. M. Johnson, S. Majd, P. Prangkio, R. C. Rollings, J. Li, J. Yang, M. Mayer, *Nat. Nanotechnol.* **2011**, *6*, 253.
[23] B. J. Hinds, *Curr. Op. Solid State Mater. Sci.* **2012**, *16*, 1.
[24] R. A. Steinbrecht, *Int. J. Insect Morphol. Embryol.* **1997**, *26*, 229.
[25] D. Losic, M. A. Cole, B. Dollmann, K. Vasilev, H. J. Griesser, *Nanotechnology* **2008**, *19*, 245704.
[26] A. Adebuer, M. M. Chehimi, I. Gallardo, J. Pinson, N. Vila, *Langmuir* **2004**, *20*, 8243.
[27] J. C. Love, L. A. Estroff, J. K. Kriebel, R. G. Nuzzo, G. M. Whitesides, *Chem. Rev.* **2005**, *105*, 1103.
[28] J. Schmitt, H. Hess, H. G. Stunnenberg, *Mol. Biol. Rep.* **1993**, *18*, 223.
[29] P. Lam, K. Kumar, G. Winek, T. M. Przybycien, *J. Electrochem. Soc.* **1999**, *146*, 2517.